THE JOURNAL OF PHYSICAL CHEMISTRY B

Article

pubs.acs.org/JPCB

Dimerization of Chirally Mutated Enkephalin Neurotransmitters: Implications for Peptide and Protein Aggregation Mechanisms

Christian Bleiholder, Nicholas F. Dupuis, and Michael T. Bowers*

Department of Chemistry and Biochemistry, University of California, Santa Barbara, California 93106, United States

Supporting Information

ABSTRACT: We have probed the structures and aggregation propensities of chirally substituted [Ala^2]-Leu-Enkephalin peptides (i.e., Leu-Enkephalin G2A) with a combination of ion-mobility spectrometry/mass spectrometry and techniques of computational chemistry. Our IMS/MS data reveal a strong correlation between the propensity to form peptide dimers and the subsequent aggregation propensity. This correlation indicates that the dimerization process is fundamental to the overall self-assembly process. Our computational data correlate a conformational conversion during the peptide association process with a reduced experimental dimer formation and subsequent aggregation propensity. Furthermore, our analysis indicates that monomer activation does not precede peptide association and thus suggests that the entire-refolding or gain-in-interaction models are more realistic accounts of the peptide self-assembly process than the monomer-conversion model. In sum, our results suggest that conformational transitions of early peptide oligomers represent bottlenecks of the peptide self-assembly process and thus highlight the importance of structurally characterizing this reaction during amyloid formation.

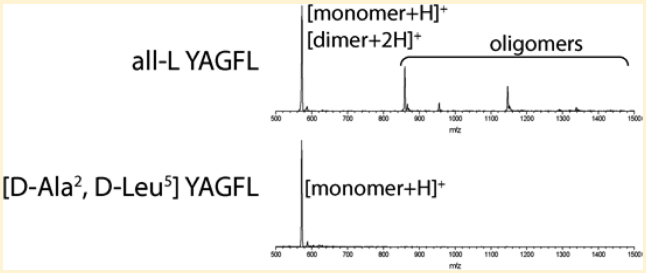

INTRODUCTION

Peptides can interact with one another and self-assemble into oligomers.[1] Peptide self-assembly into amyloid fibrils,[2,3] extracellular deposits of proteins or peptides, is particularly relevant because of the central implication of such structures in amyloid diseases such as Alzheimer's or Parkinson's diseases.[1,4−8] The discovery[9−12] that intermediate, soluble peptide oligomers are the species primarily responsible for disease pathology ("amyloid cascade hypothesis") has led to intensive research efforts aimed at elucidating the mechanistic details of early events during peptide self-assembly.[4,5,8,10,13−20] Recently, the desire to understand the mechanistic details of early events in peptide aggregation has gained greater weight because of evidence that oligomer toxicity in various amyloid diseases might be caused by a common structural motif[20,21] that might be generic to peptide assemblies.[6,7] Furthermore, recent setbacks in the development of therapeutic agents for amyloid diseases[22,23] have demonstrated that the current understanding of peptide aggregation does not provide a working framework for developing amyloid disease therapeutics.

One fundamental problem of research related to amyloid formation and disease is that only the mature aggregate and the isolated monomer are readily amenable to structural characterization by most experimental techniques.[24] However, peptide self-assembly is governed by association, dissociation, and structural conversion processes of peptide monomers and transient oligomers in a steady state with the mature aggregate,[14,25−28] such as an amyloid fibril. The amyloid cascade hypothesis suggests that these transient oligomers include the disease-causing agents, but their specific structures or abundances are not accessible by bulk measurements using traditional physicochemical techniques[15,19,29−32] that measure all oligomeric states as a single convoluted entity. In particular, conformational transitions and/or reorganization of transient, intermediate oligomers, a crucial step during the formation of β-pleated amyloid from globular monomeric proteins, are not directly amenable by bulk methods. Recently,[14] we reported the first direct observation of molecular processes that occur during the self-assembly of peptides en route to mature aggregates as soluble oligomers grow one monomer at a time using ion-mobility spectrometry/mass spectrometry (IMS/MS). These results were achieved by identifying a specific oligomeric state from a solution distribution of oligomers by mass spectrometry and subsequently determining its collision cross section by ion-mobility spectrometry.[33,34] We succeeded in directly elucidating the self-assembly mechanism of several peptides, including amyloid forming peptides,[19,29] and observed conformational transitions of early, soluble peptide oligomers from globular to fibrillar conformation, including the "steric zippers" motif of two interdigitated β-strands.[35]

Several generic nucleation−polymerization models of peptide self-assembly have been proposed based on bulk measurements. Central to these models is a conformational transition from the native peptide fold to a conformation prone to aggregation into β-pleated oligomers. In the templated assembly (TA) model,[36] larger oligomers act as templates that

Received: June 28, 2012
Revised: January 14, 2013
Published: January 16, 2013

induce conformational conversion of monomers in the rate-limiting step. Here, the conformational transition is a consequence of the monomer association process. The nucleated-conformational conversion (NCC) model[37] in essence proposes that structural transitions into β-pleated sheets are self-templated after association of oligomers (instead of monomers) to already existing structurally converted oligomers. Conformational conversion of the monomer is also rate-limiting in the monomer-directed conversion (MDC) model.[38] However, in this model, peptide association is a consequence of conformational conversion, which activates peptide monomers for their assembly into oligomers. In essence, the differences between these proposed mechanisms of amyloid peptide self-assembly can be summarized in the question of whether the required conformational conversion is the nucleation step in the amyloid formation process.

Apart from the technical difficulties of investigating a steady-state system of transient peptide oligomers by traditional techniques, any mechanistic study of peptide aggregation is further complicated by the fact that the overall assembly process can be overwhelmingly complex[8,25,31,39−41] and strongly dependent on the peptide primary sequence investigated[42,43] and solution conditions[18,44,45] such as temperature, ionic strength, and pH. However, all aggregation processes share the fact that two monomers must associate to a dimer before formation of larger oligomers is possible. Self-assembly is impossible without dimerization first, at least for all reasonable experimental conditions. The dimerization reaction of peptides is dominated by the same molecular processes that also govern the steady state of larger oligomers: association and conformational transition. First, two separated peptides must noncovalently interact with one another and associate into a dimer (association). Second, the isolated native monomer structure might differ from that of the monomer components within the dimer, so peptide monomers might be required to refold into a different structure (conformational transition). These two processes can occur simultaneously ("gain-in-interaction model")[46] or separately, with the conformational transition occurring either before association of the monomers ("monomer-refolding model")[38] or after the dimer has already been formed ("entire-refolding model").[47] Thus, the association of two peptides into a dimer is governed by the same processes as the later stages of peptide assembly in the TA, NCC, and MDC models. Therefore, a detailed investigation of the dimerization reaction will advance understanding of the processes that occur during later peptide aggregation steps.

Here, we combine IMS/MS with computational chemistry methods to correlate the overall aggregation and dimerization propensities of chirally substituted [Ala^2]-Leu-Enkephalin peptides with the structural similarity between their peptide monomers and dimers. This approach is based on the notion that amyloid formation of proteins can often be traced back to self-recognition elements of as few as five amino acid residues in length.[48,49] Much research is currently devoted to elucidating how these small fragments can be used as a starting point for aggregation inhibitors. Doig and co-workers described[48,49] how N-methylated enantiomers of these self-recognition elements from amyloid proteins can prevent self-assembly into amyloid fibrils. Moreover, heterochiral peptides and proteins in general have a strong pharmacological interest[50] and are active ingredients in medications against human immunodeficiency virus (HIV)[51,52] or Parkinson's and Alzheimer's diseases.[48,49] It is therefore of high relevance to systematically investigate how D-amino acid substitutions affect the aggregation process of peptides and, in particular, the dimerization reaction as it is the most fundamental reaction of the overall aggregation process.

MATERIALS AND SAMPLE PREPARATION

Samples were purchased from Sigma (St. Louis, MO) and used without further purification. Peptides that were not purchased through Sigma were custom synthesized by Genscript Corp. (Piscataway, NJ) at greater than 95% purity. Stock solutions were made for all samples at concentrations of 1−3 mg/mL in 50/50 methanol/water and diluted to the desired final concentrations for use in experiments. The concentrations of stock solutions were checked by UV absorbance (Beckman Coulter DU640; Fullerton, CA).

MASS SPECTROMETRY AND ION-MOBILITY INSTRUMENTATION

Ion-mobility experiments were performed on an instrument built in-house, which has been described in detail previously.[53] Briefly, the instrument consists of an electrospray source, source-ion funnel, drift tube, exit funnel, quadrupole mass analyzer, and detector. All samples are loaded into gold-coated borosilicate capillaries that have been pulled to a fine point on a tip puller (Sutter Instrument Co., Novato, CA). Ions are formed by applying a voltage to the sample tip (0.5−2.0 kV), which are then pulled into the source chamber through a small capillary. The ions are focused and stored in an hourglass-shaped ion funnel and injected into the drift tube filled with ∼13 Torr of He buffer gas. The ions are drifted through the tube under the influence of a weak electric field (5−20 V/cm) and are collected again by an exit-ion funnel, where they are transmitted through a small orifice into a high-vacuum chamber. The ions are then mass analyzed and detected with a conversion dynode and electron multiplier.

Mobility of an ion is measured by injecting a short (∼100 μs) pulse of ions into the drift tube with the quadrupole mass analyzer set to transmit only the ion of interest. The ions are then detected as a function of arrival time (t_A), generating an arrival time distribution (ATD). A reduced mobility constant (K_0) is obtained by measuring the ion-packet arrival time at varying drift voltages and accurately recording the temperature and pressure. The relationship between K_0 and t_A is given by[54]

$$K_0 = l^2 \frac{273.15}{760T} \frac{p}{V} \frac{1}{t_A - t_0} \tag{1}$$

where l is the length of the drift tube; T and p are the temperature and pressure of the buffer gas, respectively; V is the drift voltage; and t_0 is the time the ions spend outside of the drift tube. Once K_0 is measured, a collision cross section (σ) of the ion can be calculated with the equation

$$\sigma = \frac{3e}{16N_0}\left(\frac{2\pi}{\mu k_B T}\right)^{1/2} \frac{1}{K_0} \tag{2}$$

Here, T is the temperature of the buffer gas in kelvin, N_0 is the number density of He at standard temperature and pressure, z is the total charge of the ion, μ is the reduced mass of the He-ion collision system, and k_B is the Boltzmann constant.

TRAVELING-WAVE INSTRUMENTATION

The traveling-wave instrument is a prototype of the Waters Synapt High Definition Mass Spectrometer. The instrument

dx.doi.org/10.1021/jp306386p | J. Phys. Chem. B 2013, 117, 1770−1779

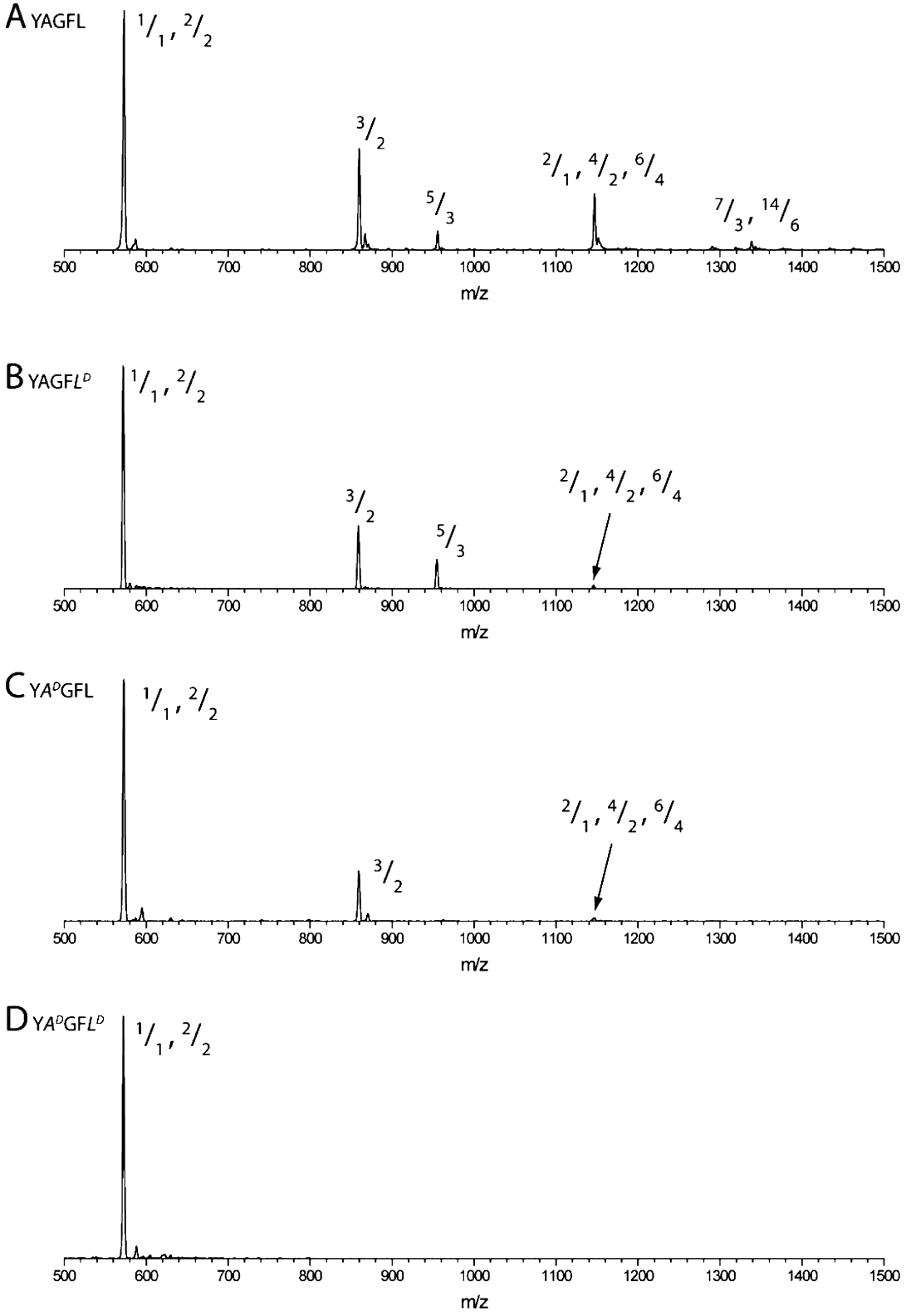

Figure 1. Electrospray ionization-quadrupole (ESI-Q) spectra for enantiomerically pure solutions of sequences (A) all-L YAGFL, (B) YAGFL^D, (C) YA^DGFL, and (D) YA^DGFL^D. Peaks are annotated with their n/z values, where n is the oligomer number (monomer = 1, dimer = 2, etc.) and z is the charge. The stronger propensity for self-assembly decreases in the order all-L YAGFL > YAGFL^D > YA^DGFL > YA^DGFL^D (i.e., with increasing degree of heterochirality).

hardware and operation are described in detail elsewhere.[55] Briefly, the instrument is a modified quadrupole time-of-flight (Q-TOF) instrument with a stacked-ring ion-guide mobility cell. The mobility cell has two key voltages. The first is a dc pulse applied to each consecutive pair of lenses. The pulse moves to each subsequent pair of lenses traveling down the length of the mobility cell, forming the traveling wave. The second voltage is a radially confining radio-frequency (RF)

dx.doi.org/10.1021/jp306386p | J. Phys. Chem. B 2013, 117, 1770−1779

voltage on one lens with the antiphase RF voltage applied to the adjacent lens. In this arrangement, the higher-mobility ions tend to stay in front of the waves, whereas the lower-mobility ions repeatedly fall back over the waves, resulting in spatial separation. Following the mobility cell, the ions are analyzed by a traditional orthogonal-acceleration time-of-flight apparatus.

COMPUTATIONAL DETAILS

Explicit-solvent molecular dynamics (MD) calculations were carried out for the dimers with the Amber-03 force field[56] in conjunction with the TIP3P water model[57] in a truncated octahedral box. The initial intermolecular distance in the dimeric systems was set to 12 Å. The minimum distance of the molecule and the box wall filled with solvent was chosen as 12 Å. A cutoff of 10 Å was chosen for nonbonded interactions, and the particle-mesh Ewald procedure[58] was applied for the treatment of periodic boundary conditions.[59] The initial geometry was relaxed prior to MD calculations using the Amber-03 force field as follows: First, a geometry optimization of the solvent molecules was performed at constant volume while fixing the geometry of the peptide. This step was followed by a geometry relaxation of the whole system, also at constant volume. Heating of the relaxed system from 0 to 300 K was performed in two stages. First, the system was propagated for 20 ps at constant volume with a restraint of 10 kcal/mol on the atomic positions of the peptides as the temperature was raised gradually to 300 K using Langevin dynamics[59] with a collision frequency of 1 ps^{-1}. This was followed by a 100-ps propagation time at constant pressure. For all MD calculations, the SHAKE algorithm[60] was utilized to remove high-frequency motions of hydrogen atoms. For each dimer system, 20 different trajectories with randomly initialized velocities were propagated for approximately 30−40 ns each in the subsequent production MD calculations, amounting to a total simulation time of approximately 600−800 ns for each sequence. To this end, randomly selected snapshots from the last 100 ps of the system initialization were used as starting geometries. Here, TIP3P was used as the solvent model, periodic boundary conditions were applied at constant pressure, and propagation at 300 K was performed by Langevin dynamics. Each 2 ps, a snapshot from the trajectory was saved for further structural analysis. For each saved snapshot, the center-of-mass distance of the two peptide monomers was computed, and the parameter optimized surfaces (POPS) algorithm[61] was utilized to partition the solvent-accessible surface area into hydrophilic and hydrophobic contributions. Based on the center-of-mass distance (d_{COM}) between the two peptide units, each snapshot was defined as monomer (d_{COM} > 24 Å), dimer (d_{COM} < 14 Å), or transition state (14 Å < d_{COM} ≤ 24 Å). These values were chosen based on the frequency distribution $f(d_{COM})$ of the center-of-mass distance d_{COM} (see the Supporting Information, section S1). The POPS algorithm was used to compute solvent-accessible surface areas (SASAs) and solvation free energies ΔG_{solv} according to eq 3 as defined previously[61]

$$\Delta G_{solv} = \sigma^{Phob}\Delta A^{Phob} - \sigma^{Phil}\Delta A^{Phil} \quad (3)$$

Here, ΔA^{Phob} and ΔA^{Phil} are the hydrophobic and hydrophilic solvent-accessible surface areas, respectively, and σ^{Phob} = 12 cal mol^{-1} $Å^{-2}$ and σ^{Phil} = 60 cal mol^{-1} $Å^{-2}$.[61] This protocol has been successfully used to partition the solvation free energy into hydrophobic and hydrophilic contributions and was applied to identify key interactions in the ribosome.[61]

The strength of interaction between two chains in a dimer complex was evaluated by computing ΔG_{int} as defined in this work by

$$\begin{aligned}\Delta G_{int} &= \Delta\Delta G_{solv}\\ &= \Delta\Delta G_{int}^{Phob} + \Delta\Delta G_{int}^{Phil}\\ &= \sigma^{Phob}(\Delta A_{A+B}^{Phob} - \Delta A_{A}^{Phob} - \Delta A_{B}^{Phob})\\ &\quad - \sigma^{Phil}(\Delta A_{A+B}^{Phil} - \Delta A_{A}^{Phil} - \Delta A_{B}^{Phil})\end{aligned} \quad (4)$$

Here, the interaction energy, ΔG_{int}, is defined as the difference in solvent free energy $\Delta\Delta G_{solv}$ between the dimer complex (ΔA_{A+B}^{Phob} and ΔA_{A+B}^{Phil} are the hydrophobic and hydrophilic solvent-accessible surface areas, respectively, of the dimer) and the isolated monomer chains in the same geometry as in the dimer ($\Delta A_{A,B}^{Phob}$ and $\Delta A_{A,B}^{Phil}$ are the corresponding hydrophobic and hydrophilic solvent-accessible surface areas). This definition of the interaction energy thus reflects the magnitude of the interaction caused by the penetration of the molecular surfaces of the two units A and B within the dimer complex and follows established conventions in the theory of intermolecular interactions.[62,63] Values can be found in Table S1 in the Supporting Information.

RESULTS AND DISCUSSION

The endogenous peptide neurotransmitter Leu-Enkephalin contains three chiral centers in its amino acid sequence YGGFL. The synthetic analogues [Ala^2]-Leu-Enkephalin with sequence YAGFL contain four chiral residues (Tyr, Ala, Phe, Leu) that can be individually stereoinverted, resulting in three families with varying degree of heterochirality (see Scheme S1, Supporting Information). Family 1 consists of the two homochiral peptides all-L and all-D YAGFL. Family 2 contains the eight peptides with a single chiral mutation with respect to the all-L and all-D forms. Family 3 consists of six peptide sequences in which two residues with L configuration are mixed with two residues of D configuration. In this work, we study the self-oligomerization of the peptides all-L/all-D YAGFL (family 1), $YA^DGFL/Y^DAGF^DL^D$, $YAGFL^D/Y^DA^DGF^DL$ (family 2), and YA^DGFL^D/Y^DAGF^DL (family 3). For brevity, we restrict the discussion of our results to one enantiomeric peptide sequence only.

Figure 1 shows ESI-Q mass spectra recorded for the homochiral peptide all-L YAGFL and the heterochiral peptides YA^DGFL and $YAGFL^D$ (both from family 2) and YA^DGFL^D (family 3). The figure reveals significantly different self-assembly processes, and we note that the propensity for self-assembly strongly decreases with increasing sequence heterochirality. The homochiral sequence all-L YAGFL displays significant formation of oligomers larger than the dimer (Figure 1A), such as n/z 3/2 (m/z 855.4), n/z 4/2 (m/z 1140.3), n/z 6/4 (m/z 1140.3), n/z 5/3 (m/z 950.4), n/z 7/3 (m/z 1330.2), n/z 9/4 (m/z 1282.7), and n/z 12/5 (m/z 1368.2). (Oligomers are denoted by their n/z ratios, where n denotes the number of monomer units within the oligomer and z is the overall charge state.) These peaks are identified based on their unique and unambiguous m/z values. There is a general level of background counts in the mass spectrum above m/z 1250, which suggests the existence of higher-order peptide clusters in the sample that the quadrupole on this instrument is not able to resolve. However, the high mass resolution of the ESI-Q-TOF instrument clearly indicates the existence of oligomeric states up to at least 30mers (Figure S2 in the Supporting

dx.doi.org/10.1021/jp306386p | J. Phys. Chem. B 2013, 117, 1770−1779

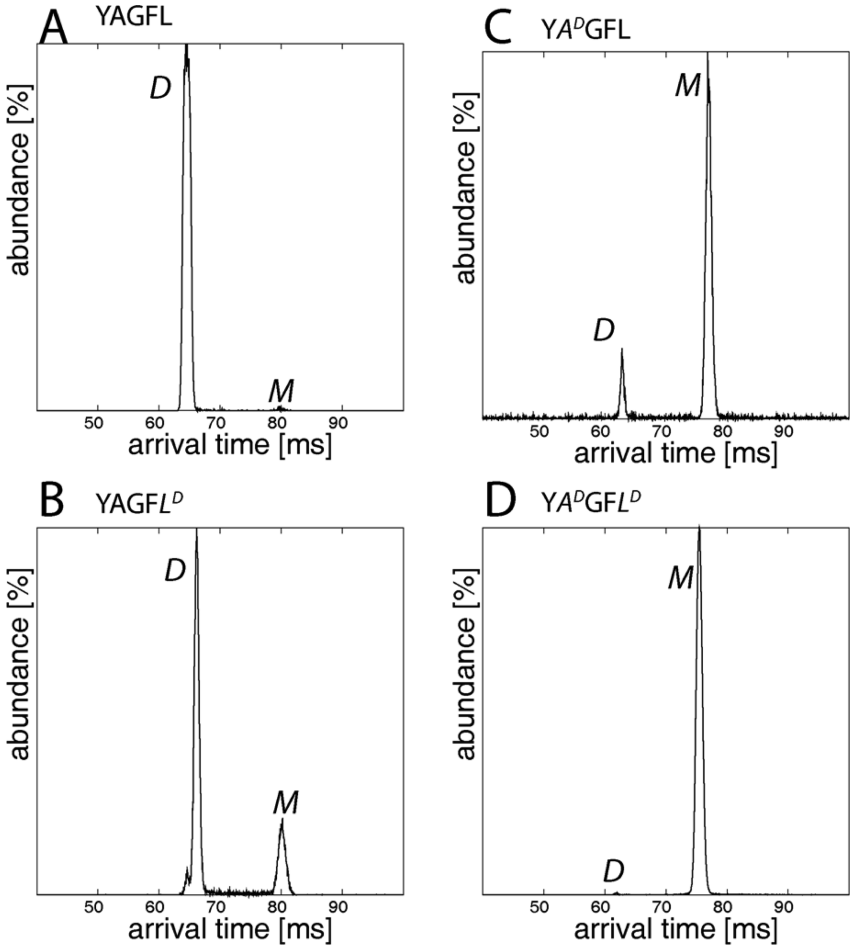

Figure 2. Arrival time distributions (ATDs) of the n/z 1/1 (m/z 570) peaks of sequences (A) all-L YAGFL, (B) YAGFL^D, (C) YA^{D}GFL, and (D) YA^{D}GFL^D. The ATDs display two features: The earlier one (arrival time of approximately 65 ms) comprises peptide dimers (D, n/z 2/2), and the later one (arrival time of approximately 80 ms) comprises peptide monomers (M, n/z 1/1). We note that the dimer-to-monomer ratio r decreases in the series all-L YAGFl > YAGFL^D > YA^{D}GFL > YA^{D}GFL^D (i.e., with increasing degree of heterochirality).

Information). Self-oligomerization of YA^{D}GFL^D (Figure 1D) is significantly diminished when compared to that of all-L YAGFL. Here, only the monomer peak (m/z 570) is clearly visible in the ESI-Q spectrum. The two heterochiral peptides YAGFL^D and YA^{D}GFL from family 2 with one D-amino acid residue display an intermediate extent of self-assembly, with the former undergoing assembly somewhat faster than the latter. Overall, we note a substantial influence of sequence heterochirality on the overall aggregation propensity. This observation supports the view[64] that chirally substituted peptides are a viable option to alter the kinetics of peptide self-assembly processes.

The differences in the overall self-oligomerization propensity among the various chiral alloforms discussed above is reflected in the arrival time distributions (ATDs) of the n/z 1/1 (m/z 570) peak for the corresponding sequence (see Figure 2). These data were recorded at 25 μM, where strong monomer signal was obtained but the contribution of higher-order oligomers to the mass spectrum was minimal. Two main features are visible in the ATDs, with the shorter drift time feature corresponding to the doubly protonated dimer peak (n/z 2/2 at approximately 65 ms) and the longer drift time feature representing the singly protonated monomer peak (n/z 1/1 at approximately 80 ms). These features were previously identified based on their individual ^{13}C isotope distributions.[53] The relative abundance ratios of the monomer and dimer species are listed in Table 1. The ATDs obtained for the homochiral peptides all-L and all-D YAGFL (Figure 2A and Figure S3 in the Supporting Information) show a prevailing n/z 2/2 dimer feature, whereas the n/z 1/1 monomer feature is visible at much smaller intensity. The value for the dimer-to-monomer ratio of r = 24.4 demonstrates that the base peak in Figure 1A consists mainly of dimer. This observation is in strong contrast to the ATD for the peptide YA^{D}GFL^D (Figure 2D), for which the n/z 1/1 base peak at m/z 570 shows only marginal dimer population and mainly consists of the monomer (r = 0.1). The heterochiral sequence YAGFL^D (r = 4.4, Figure 2B) shows prevailing formation of dimer, but the monomer peak is stronger than for all-L YAGFL (r = 24.4, Figure 2A). The ATD of YA^{D}GFL (r = 0.5, Figure 2C) indicates a smaller

Table 1. Experimental Dimer-to-Monomer Ratio r and Computed Structural Parity ρ for the Various Peptide Sequences Investigated

sequence	r	ρ
all-L YAGFL	24.4	5.36395×10^{-8}
YAGFL^D	4.4	2.64353×10^{-8}
YA^{D}GFL	0.5	2.18118×10^{-8}
YA^{D}GFL^D	0.1	1.57398×10^{-8}

dx.doi.org/10.1021/jp306386p | J. Phys. Chem. B 2013, 117, 1770−1779

dimerization propensity than for YAGFL^D, with a prevailing monomer peak and only a minor contribution from the dimer. These findings clearly indicate a strong correlation of the overall propensity to form higher-order oligomers (Figure 1) with the propensity for dimer formation (Figure 2).

Figure 3A correlates the dimer-to-monomer ratio r in the n/z 1/1 (m/z 570) ATDs (see Table 1) with the D-amino acid content h for each peptide [with $h = n_D/(n_D + n_L)$, where n_D and n_L are the numbers of D- and L-amino acids, respectively]. The data points for the peptides with one and three D-amino acids display some differences in dimer-to-monomer ratio r depending on the location of the chiral substitution in the peptide [i.e., Ala(2) or Leu(5)], but the differences are small with respect to the overall trend observed in Figure 3A. The data show that the degree of dimerization is maximal when the peptides are homochiral (r = 24.4 for all-L YAGFL). It is also evident that the propensity to dimerize is reduced by introducing chirally substituted amino acids into the peptide (r = 4.4, 0.5, and 0.1 for YAGFL^D, YA^{D}GFL, and YA^{D}GFL^D, respectively; see Table 1). Therefore, our data clearly indicate that the dimerization propensity (Figure 2) correlates well with the overall aggregation propensity (Figure 1), providing support that the dimerization reaction is fundamental to the overall aggregation process.

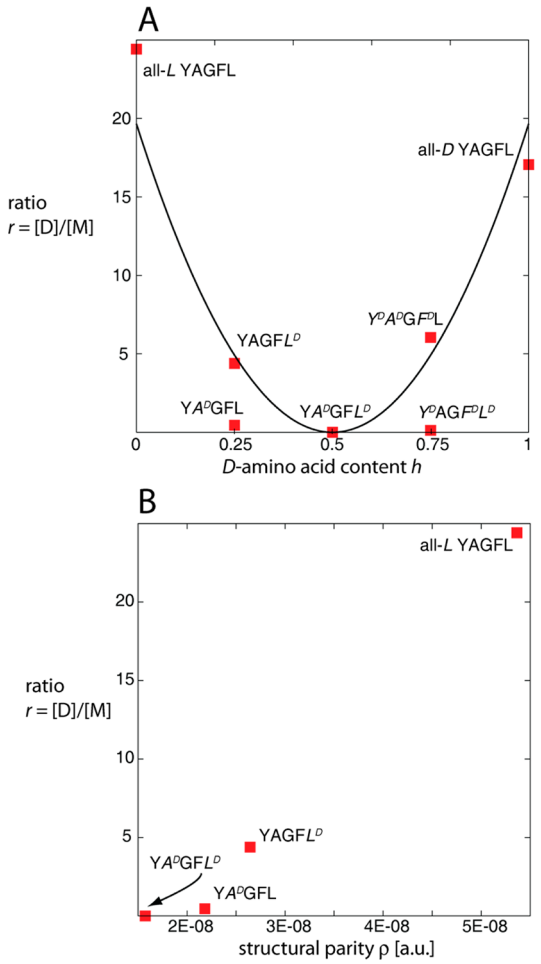

Figure 3. (a) Ratio r of dimer to monomer abundances in the n/z 1/1 peaks (m/z 570) of various YAGFL species as a function of the D-amino acid content $h = n_D/(n_D + n_L)$ for each peptide (n_D and n_L denote the numbers of D and L-amino acid residues, respectively). Note that h does not denote the degree of racemization and that the sample solutions are enantiopure. (b) Correlation between the ratio r of dimer to monomer abundances in the n/z 1/1 peaks (m/z 570) and the structural parity ρ computed from our molecular dynamics simulations for the peptides investigated (see eq S3 in the Supporting Information). We note that a higher value for the structural parity ρ (reflecting a stronger structural similarity between monomer, transition-state, and dimer structures) correlates with a larger value for r.

The correlation between the experimental dimer-to-monomer ratio r observed in the n/z 1/1 ATD and the computed structural parity ρ (see eq S1 in the Supporting Information) based on our molecular dynamics simulations is depicted in Figure 3B. Figure 3B shows that a higher experimental dimer-to-monomer ratio r correlates with a higher computed structural parity ρ. This correlation indicates that a higher experimental dimer-to-monomer ratio r (and thus overall aggregation propensity) is observed for those peptide sequences that display a stronger structural similarity between the monomer, transition-state, and dimer structures (larger value of ρ). In other words, peptide sequences subjected to a conformational change when forming a dimer display a weaker experimental aggregation propensity than those sequences that do not require such a structural transition. Therefore, our data suggest that conformational conversion processes represent bottlenecks or free energy maxima of the peptide self-assembly process.

Figure 4 displays the relative populations of different peptide conformations as the two peptide chains associate to form a dimer as observed in our dimer MD simulations. Each of the two peptide chains in our dimer simulations can adopt compact or extended conformations. Thus, three different possible combinations of chain conformations are observed in our dimer simulation. First, both monomer chains can take on extended conformations simultaneously ($d^1_{C,N}$, $d^2_{C,N}$ > 7.0 Å, denoted as *ee* conformation). Second, both monomer chains can exist in compact conformations $d^1_{C,N}$, $d^2_{C,N}$ < 7.0 Å, denoted as *cc* conformation). Finally, one peptide chain can adopt an extended and one a compact conformation (denoted as *ce* conformation). We note that *ee* conformations strongly prevail for the peptides all-L YAGFL (Figure 4A) and YAGFL^D (Figure 4B). Here, *ee* conformations represent more than 75% (all-L YAGFL) and 65% (YAGFL^D) at any point of the association process. We note that, especially at small intermolecular distances (center-of-mass distance $d_{COM} \leq$ 10−15 Å), *ee* dimer conformations prevail. Whereas *cc* conformations are negligible for all-L YAGFL and YAGFL^D, *ce* conformations are observed at larger intermolecular center-of-mass distances (i.e., $d_{COM} \geq$ 10−15 Å) but are negligible at small center-of-mass distances ($d_{COM} \leq$ 10−15 Å). We thus observe no profound conformational transition during the dimer formation of all-L YAGFL and YAGFL^D.

In contrast, extended *ee* conformations prevail for the peptide YA^{D}GFL^D and possibly YA^{D}GFL only at intermolecular distances of $d_{COM} \leq$ 10−15 Å, but *ce* conformations are equally populated for distances of d_{COM} > 15−20 Å. Compact *cc* conformations are observed, but only for distances of d_{COM} > 20−25 Å. The data thus indicate a substantial conformational conversion from an equidistribution of *ee* and *ce* conformations for the separated monomers to prevailing *ee* conformations in the aggregated dimer state of YA^{D}GFL^D and possibly YA^{D}GFL. The *ee* dimer conformations for YA^{D}GFL^D become favored in the transition-state regime ($d_{COM} \approx$ 15−25 Å) as the center-of-mass distance d_{COM} decreases. Consequently, the data suggest

dx.doi.org/10.1021/jp306386p | J. Phys. Chem. B 2013, 117, 1770−1779

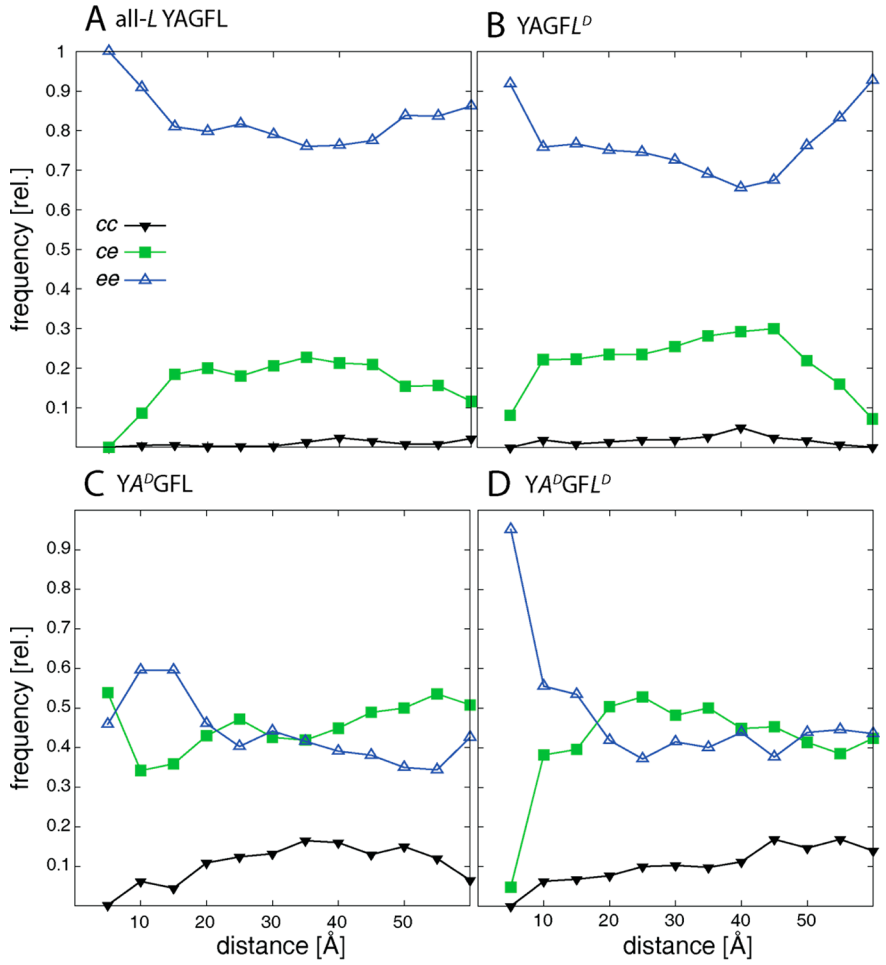

Figure 4. Relative populations of conformations of extended (*ee*), compact (*cc*), and mixed (*ce*) conformations as a function of the center-of-mass distance of the two peptide chains. We note only minor changes in relative population for the strongly aggregating sequences (A) all-L YAGFL and (B) YAGFL^D. Significant changes in the prevailing conformation are observed for (C) YA^{D}GFL and (D) YA^{D}GFL^D.

that strengthening of the initially weak contact between two YA^{D}GFL^D peptide chains occurs simultaneously with conformational change during the transition state of the dimerization reaction.

The driving force underlying the prevalence of *ee* dimer conformations observed in our simulations (Figure 4) can be evaluated by comparing the differences between *ee* and *ce* conformations in hydrophilic (ΔG_{int}^{Phil}) and hydrophobic (ΔG_{int}^{Phob}) contributions to the dimer interaction energy (see Figure 5, as well as Table S1 in the Supporting Information). Figure 5A displays the difference $\Delta\Delta G_{int}^{ee,ce} = \Delta G_{int}^{ee} - \Delta G_{int}^{ce}$ in interaction free energy between *ee* and *ce* dimer conformations as a function of the intermolecular distance d_{COM} up to 20 Å for the peptide sequences studied. Overall, the increasingly negative values for $\Delta G_{int}^{ee,ce}$ show that *ee* conformations become increasingly more strongly bound than *ce* conformations with decreasing intermolecular distance. The only exception to this trend is the sequence YA^{D}GFL for the shortest distances (see Figure 4), and this might be due to sampling error. Thus, on a qualitative basis, the analysis of the interaction energy accounts for the prevalence of *ee* conformations observed for the dimer states in Figure 4.

Panels B and C of Figure 5 display the differences in hydrophilic ($\Delta G_{int}^{Phil} = \Delta G_{int}^{Phil,ee} - \Delta G_{int}^{Phil,ce}$) and hydrophobic ($\Delta\Delta G_{int}^{Phob} = \Delta G_{int}^{Phob,ee} - \Delta G_{int}^{Phob,ce}$) contributions to the interaction energies of *ee* and *ce* conformations. The data reveal that hydrophilic (i.e., hydrogen-bonding or charge−charge) interactions contribute significantly more strongly to *ee* than *ce* dimers of all-L YAGFL and YA^{D}GFL^D, whereas they appear to be similarly important for *ee* and *ce* dimers of YAGFL^D and YA^{D}GFL (Figure 5B). This observation suggests that mainly hydrophilic interactions are responsible for the conformational transition of YA^{D}GFL^D. Hydrophobic interactions (see Figure 5C) are clearly more prevalent in *ce* than *ee* dimers of all-L YAGFL, and they are responsible for the strong prevalence of *ee* dimers for YAGFL^D. The analysis further reveals that hydrophobic contacts slightly favor *ee* conformations for YA^{D}GFL.

In sum, our analysis of the interaction energies suggests that the conformational conversion in YA^{D}GFL^D is caused by strong hydrophilic interactions present in the *ee* dimer conformation. For YA^{D}GFL, both hydrophilic and hydrophobic interactions slightly favor *ee* dimer conformations. In the discussion of our computational data above (see Figure 4), we noted a transition from compact (*ce*) to extended (*ee*) dimer conformations for YA^{D}GFL^D and possibly also for YA^{D}GFL. The conversion from *ce* to *ee* conformations is particularly prominent for the regime of the aggregated dimer state, but our analysis also indicates that the conformational change is initiated during the dimerization transition state. No such structural change is observed for all-L YAGFL and YAGFL^D. Here, *ee* conformations prevail throughout the whole association process, but again

dx.doi.org/10.1021/jp306386p | J. Phys. Chem. B 2013, 117, 1770−1779

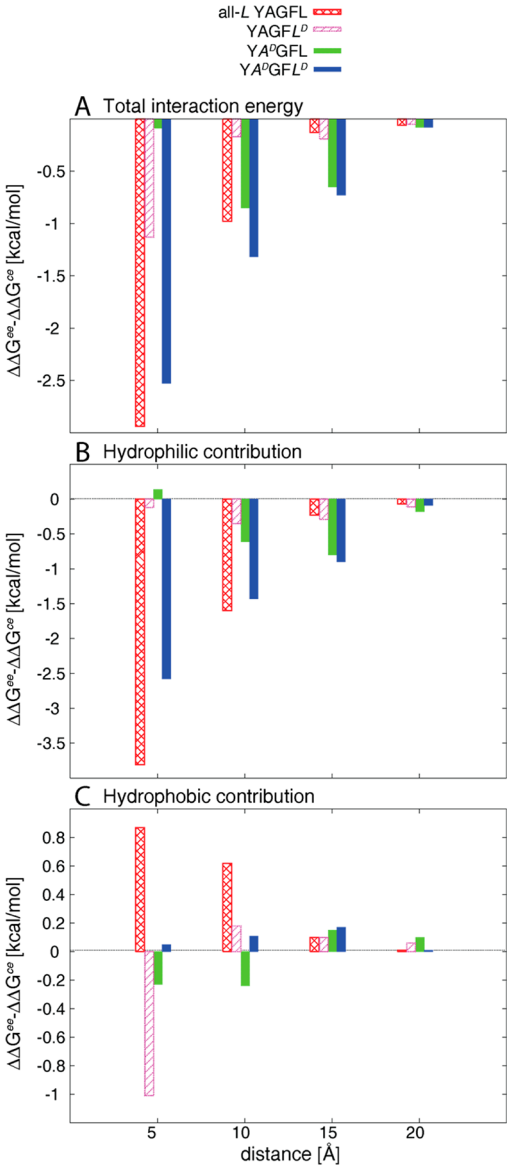

Figure 5. Difference in interaction energy $\Delta\Delta G_{int} = \Delta G^{ee}_{int} - \Delta G^{ce}_{int}$ bewteen *ee* and *ce* conformations as a function of the intermolecular distance d_{COM} for the peptide sequences studied. Negative values of $\Delta\Delta G_{int}$ indicate preference for *ee* conformations. (A) Total interaction energy indicates that, with decreasing intermolecular distance d_{COM}, peptides in *ee* dimer conformations interact more strongly than *ce* dimers. (B) Dimers in *ee* conformation display a stronger hydrophilic interaction than dimers in *ce* conformations. (C) Hydrophobic interactions favor the *ce* conformations for all-L YAGFL and YA^DGFL^D but the *ee* conformation for YA^DGFL and $YAGFL^D$.

especially for distances of $d_{COM} \leq 15$ Å. Cluster analysis of the snapshots sampled during MD simulations of the dimer formation process (see Figure S5 in the Supporting Information) reveals that the two peptide chains start to associate with each other through weak hydrophilic and/or hydrophobic contacts during the dimerization transition state (i.e., for distances of $d_{COM} \approx 15-25$ Å). Also, we note that *ee* conformations become amplified during this intermediate stage of the assembly process for YA^DGFL^D (see Figure 4 and Figure S5 in the Supporting Information). The cluster analysis reveals that the interchain bonding is then further strengthened by forming multiple noncovalent bonds in the dimer states ($d_{COM} \leq 10$ Å). This increased interaction within the dimer states of the peptide sequences studied here is accomplished by extended peptide conformations that enable multiple noncovalent contacts between the two peptide chains through an increased surface area of interaction.

Implications for Amyloid Assembly Pathways. Different mechanistic models of the peptide dimer formation reaction exist and differ from each other in the order of the association and structural conversion processes (see Scheme 1). The monomer-conversion model[38] proposes that the structural conversion takes place before the association of the monomer peptides, whereas structural conversion follows peptide association in the entire-refolding model.[47] The gain-in-interaction model[46] assumes that structural conversion and noncovalent association into the dimer complex occur in concert. Our analysis in the preceding section indicates that no conformational changes occur for the separated monomers and thus mitigates against the monomer-refolding paradigm. Instead, we note that the driving force for the *ce*-to-*ee* structural conversion observed for YA^DGFL^D relies on a structural relaxation from the initially formed dimer into a more stable dimer geometry after a weak noncovalent interaction is established in the transition-state region. Thus, a combination of the gain-in-interaction and entire-refolding models provides the best account for the dimerization process of YA^DGFL^D (see Scheme 1).

Scheme 1. Association and Conformational Conversion Steps Differ in Mechanistic Models of the Dimerization Reaction[a]

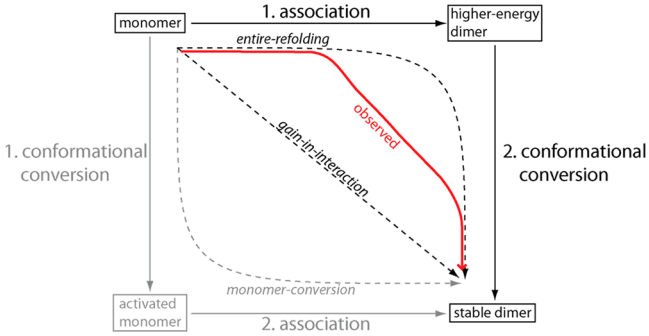

[a]Our data indicate that the conformational conversion of YA^DGFL^D is initiated by formation of weak noncovalent contacts but then occurs abruptly once a dimer has formed. Therefore, the monomer-conversion model does not provide an accurate description of the dimerization reaction investigated.

In the following discussion, we extrapolate our conclusions on the peptide dimerization reaction to the subsequent peptide assembly process and amyloid formation. An entire-refolding event of an oligomeric species becomes increasingly difficult with increasing oligomer size, because of increasing difficulties in the concerted reorganization of a larger peptide oligomer into a different quaternary structure. In particular, this applies to conversion from a random coil into a fibrillar β-strand oligomer conformation. The preceding analysis implies that structural conversion processes in amyloid formation are likely to occur at an earlier rather than later oligomer stage. This inference is in line with our recent IMS/MS study on the self-assembly pathways of several peptides, including those forming amyloid fibrils.[14] We suggest that conformational conversion into β-oligomers proceeds after association of monomeric and/

dx.doi.org/10.1021/jp306386p | J. Phys. Chem. B 2013, 117, 1770−1779

or small oligomeric species. Subsequently, these β-oligomers add and conformationally convert monomers or small oligomers to form fibrillar aggregates. Of course, this process will depend on the size and primary sequence of the peptides studied. For example, $A\beta_{1-42}$ forms non-β-sheet dodecamers that are metastable and that might be the key species that isomerizes into a β-sheet-rich oligomer.[5] In the 37-residue human IAPP peptide, however, it appears that this process occurs much earlier on.[16,44] Similarly, $A\beta_{1-40}$ isomerizes by a different route than $A\beta_{1-42}$ and might begin β-sheet formation as early as the tetramer.[65] The detailed factors that govern these native β-sheet transitions are still actively being investigated. However, the very detailed studies described here for the chirally substituted YAGFL family of peptides provide important insights into the processes that might be occurring in any aggregating system.

SUMMARY AND CONCLUSIONS

The self-assembly process of chirally substituted [Ala^2]-Leu-Enkephalin peptides was studied by a combination of ion-mobility spectrometry/mass spectrometry (IMS/MS) and computational chemistry methods. Our IMS/MS data reveal a strong correlation between the propensity to form peptide dimers and the propensity for subsequent aggregation. This correlation indicates that the dimerization process is fundamental to the overall self-assembly process. Our analysis suggests that conformational transitions are likely nucleation steps during amyloid formation. Our analysis further suggests that, for many systems, monomer activation might not precede intermolecular association of peptide chains and that the entire-refolding and gain-in-interaction models are more realistic paradigms of the peptide self-assembly process than the monomer-conversion model for most systems. We propose that amyloid formation proceeds by conformational conversion of smaller oligomeric species that subsequently associate. These larger oligomers then grow by adding and conformationally converting monomers to give fibrillar aggregates.

ASSOCIATED CONTENT

Supporting Information

Mass spectra and arrival time distributions of systems studied in this work. Definition of the structural parity ρ and analysis of the computational studies. This material is available free of charge via the Internet at http://pubs.acs.org.

AUTHOR INFORMATION

Corresponding Author

*E-mail: bowers@chem.ucsb.edu.

Notes

The authors declare no competing financial interest.

ACKNOWLEDGMENTS

This work was supported by National Science Foundation Grant CHE-090974 (M.T.B.). C.B. was supported in part by a Feodor Lynen Fellowship of the Alexander von Humboldt Foundation. M.T.B. also thanks Waters Corporation for the donation of a Synapt prototype instrument used for part of the work presented here. Support from Hewlett-Packard to the CNSI Computer Facilities is gratefully acknowledged. We are grateful S. Anderson and T. Wyttenbach for commenting on the manuscript.

REFERENCES

(1) Chiti, F.; Dobson, C. M. *Annu. Rev. Biochem.* **2006**, *75*, 333−366.
(2) Sipe, J. D. *Amyloid Proteins*; Wiley-VCH: Weinheim, Germany, 2005.
(3) Nelson, R.; Eisenberg, D. *Fibrous Proteins* **2006**, *73*, 235−282.
(4) Ehrnhoefer, D. E.; Bieschke, J.; Boeddrich, A.; Herbst, M.; Masino, L.; Lurz, R.; Engemann, S.; Pastore, A.; Wanker, E. E. *Nat. Struct. Biol.* **2008**, *15*, 558−566.
(5) Bernstein, S. L.; Dupuis, N. F.; Lazo, N. D.; Wyttenbach, T.; Condron, M. M.; Bitan, G.; Teplow, D. B.; Shea, J.-E.; Ruotolo, B. T.; Robinson; Bowers, M. T. *Nat. Chem.* **2009**, *1*, 326−331.
(6) Bucciantini, M.; Giannoni, E.; Chiti, F.; Baroni, F.; Formigli, L.; Zurdo, J. S.; Taddei, N.; Ramponi, G.; Dobson, C. M.; Stefani, M. *Nature* **2002**, *416*, 507−511.
(7) Baglioni, S.; Casamenti, F.; Bucciantini, M.; Luheshi, L. M.; Taddei, N.; Chiti, F.; Dobson, C. M.; Stefani, M. *J. Neurosci.* **2006**, *26*, 8160−8167.
(8) Kodali, R.; Wetzel, R. *Curr. Opin. Struct. Biol.* **2007**, *17*, 48−57.
(9) Kirkitadze, M. D.; Bitan, G.; Teplow, D. B. *J. Neurosci. Res.* **2002**, *69*, 567−577.
(10) Haass, C.; Selkoe, D. J. *Nat. Rev. Mol. Cell Biol.* **2007**, *8*, 101−112.
(11) Georganopoulou, D. G.; Chang, L.; Nam, J.-M.; Thaxton, C. S.; Mufson, E. J.; Klein, W. L.; Mirkin, C. A. *Proc. Natl. Acad. Sci. U.S.A.* **2004**, *102*, 2273−2276.
(12) Lambert, M. P.; Barlow, A. K.; Chromy, B. A.; Edwards, C.; Freed, R.; Liosatos, M.; Morgan, T. E.; Rozovsky, I.; Trommer, B.; Viola, K. L.; Wals, P.; Zhang, C.; Finch, C. E.; Krafft, G. A.; Klein, W. L. *Proc. Natl. Acad. Sci. U.S.A.* **1998**, *95*, 6448−6453.
(13) Woods, L. A.; Platt, G. W.; Hellewell, A. L.; Hewitt, E. W.; Homans, S. W.; Ashcroft, A. E.; Radford, S. E. *Nat. Chem. Biol.* **2011**, *7*, 730−739.
(14) Bleiholder, C.; Dupuis, N. F.; Wyttenbach, T.; Bowers, M. T. *Nat. Chem.* **2011**, *3*, 172−177.
(15) Shima, S.-H.; Guptab, R.; Linga, Y. L.; Strasfelda, D. B.; Raleigh, D. P.; Zannia, M. T. *Proc. Natl. Acad. Sci. U.S.A.* **2009**, *106*, 6614−6619.
(16) Dupuis, N. F.; Wu, C.; Shea, J. E.; Bowers, M. T. *J. Am. Chem. Soc.* **2009**, *131*, 18283−18292.
(17) Wang, J. T., C.; Chen, H.-F.; Luo, R. *Biophys. J.* **2008**, *95*, 5037−5047.
(18) Chiti, F.; Dobson, C. M. *Nat. Chem. Biol.* **2008**, *5*, 15−21.
(19) Sawaya, M. R.; Sambashivan, S.; Nelson, R.; Ivanova, M. I.; Sievers, S. A.; Apostol, M. I.; Thompson, M. J.; Balbirnie, M.; Wiltzius, J. J. W.; MacFarlane, H. T.; Madsen, A. Ø.; Riekel, C.; Eisenberg, D. *Nature* **2007**, *447*, 453−457.
(20) Kayed, R.; Head, E.; Sarsoza, F.; Saing, T.; Cotman, C. W.; Necula, M.; Margol, L.; Wu, J.; Breydo, L.; Thompson, J. L.; Rasool, S.; Gurlo, T.; Butler, P.; Glabe, C. G. *Mol. Neurodegen.* **2007**, *2*, 18.
(21) Kayed, R.; Head, E.; Thompson, J. L.; McIntire, T. M.; Milton, S. C.; Cotman, C. W.; Glabe, C. G. *Science* **2003**, *300*, 486−489.
(22) Sevigny, J. J.; Ryan, J. M.; van Dyck, C. H.; Peng, Y.; Lines, C. R.; Nessly, M. L. *Neurology* **2008**, *71*, 1702−1708.
(23) *Nat. Med.* **2011**, *17*, 932−933.
(24) Buell, A. K.; Esbjörner, E. K.; Riss, P. J.; White, D. A.; Aigbirhio, F. I.; Toth, G.; Welland, M. E.; Dobson, C. M.; Knowles, T. P. J. *Phys. Chem. Chem. Phys.* **2011**, *13*, 20044−20052.
(25) Morris, A. M.; Watzky, M. A.; Finke, R. G. *Biochim. Biophys. Acta* **2009**, *1794*, 375−397.
(26) Auer, S.; Dobson, C. M.; Vendruscolo, M.; Maritan, A. *Phys. Rev. Lett.* **2008**, *101*, 258801.
(27) Eisenberg, D.; Nelson, R.; Sawaya, M. R.; Balbirnie, M.; Sambashivan, S.; Ivanova, M. I.; Madsen, A. O.; Riekel, C. *Acc. Chem. Res.* **2006**, *39*, 568−575.
(28) Bernstein, S. L.; Wyttenbach, T.; Baumketner, A.; Shea, J.-E.; Bitan, G.; Teplow, D. B.; Bowers, M. T. *J. Am. Chem. Soc.* **2005**, *127*, 2075−2084.
(29) Nelson, R.; Sawaya, M. R.; Balbirnie, M.; Madsen, A. Ø.; Riekel, C.; Grothe, R.; Eisenberg, D. *Nature* **2005**, *435*, 773−778.

(30) Wiltzius, J. J. W.; Sievers, S. A.; Sawaya, M. R.; Cascio, D.; Popov, D.; Riekel, C.; Eisenberg, D. *Protein Sci.* **2008**, *17*, 1467−1474.
(31) Knowles, T. P. J.; Smith, J. F.; Devlin, G. L.; Dobson, C. M.; Welland, M. E. *Nanotechnology* **2007**, *18*, 1−5.
(32) Eichner, T.; Kalverda, A. P.; Thompson, G. S.; Homans, S. W.; Radford, S. E. *Mol. Cell* **2011**, *41*, 161−172.
(33) Teplow, D. B.; Lazo, N. D.; Bitan, G.; Bernstein, S.; Wyttenbach, T.; Bowers, M. T.; Baumketner, A.; Shea, J.-E.; Urbanc, B.; Cruz, L.; Borreguero, J.; Stanley, H. E. *Acc. Chem. Res.* **2006**, *39*, 635−645.
(34) Wyttenbach, T.; Bowers, M. T. *Top. Curr. Chem.* **2003**, *225*, 207−232.
(35) Nelson, R.; Eisenberg, D. *Curr. Opin. Struct. Biol.* **2006**, *16*, 260−265.
(36) Griffith, J. *Nature* **1967**, *215*, 1043−1044.
(37) Serio, T. R.; Cashikar, A. G.; Kowal, A. S.; Sawicki, G. J.; Moslehi, J. J.; Serpell, L.; Arnsdorf, M. F.; Lindquist, S. L. *Science* **2000**, *289*, 1317−1321.
(38) Prusiner, S. B. *Science* **1982**, *216*, 136−144.
(39) Wetzel, R.; Shivaprasad, S.; Williams, A. D. *Biochemistry* **2007**, *46*, 1−10.
(40) Thirumalai, D.; Klimov, D. K.; Dima, R. I. *Curr. Opin. Struct. Biol.* **2003**, *13*, 146−159.
(41) Diaz-Avalos, R.; Long, C.; Fontano, E.; Balbirnie, M.; Grothe, R.; Eisenberg, D.; Caspar, D. L. D. *J. Mol. Biol.* **2003**, *330*, 1165−1175.
(42) Fernandez-Escamilla, A. M.; Rousseau, F.; Schymkowitz, J.; Serrano, L. *Nat. Biotechnol.* **2004**, *22*, 1302−1306.
(43) Murphy, R. M. *Annu. Rev. Biomed. Eng.* **2002**, *4*, 155−174.
(44) Dupuis, N. F.; Wu, C.; Shea, J.-E.; Bowers, M. T. *J. Am. Chem. Soc.* **2011**, *133*, 7240−7243.
(45) Calamai, M.; Chiti, F.; Dobson, C. M. *Biophys. J.* **2005**, *89*, 4201−4210.
(46) Ivanova, M. I.; Sawaya, M. R.; Gingery, M.; Attinger, A.; Eisenberg, D. *Proc. Natl. Acad. Sci. U.S.A.* **2004**, *101*, 10584−10589.
(47) Jimenez, J. L.; Nettleton, E. J.; Bouchard, M.; Robinson, C. V.; Dobson, C. M.; Saibil, H. R. *Proc. Natl. Acad. Sci. U.S.A.* **2002**, *99*, 9196−9201.
(48) Amijee, H.; Madine, J.; Middleton, D. A.; Doig, A. J. *Biochem. Soc. Trans.* **2009**, *37*, 692−696.
(49) Mason, J. M.; Kokkoni, N.; Stott, K.; Doig, A. J. *Curr. Opin. Struct. Biol.* **2003**, *13*, 526−532.
(50) Sela, M.; Zisman, E. *FASEB J.* **1997**, *11*, 449−456.
(51) Pritsker, M.; Jones, P.; Blumenthal, R.; Shai, Y. *Proc. Natl. Acad. Sci. U.S.A.* **1998**, *95*, 7287−7292.
(52) Munroe, J. E.; Shepherd, T. A.; Jungheim, L. N.; Hornhad, W. J.; Hatch, S. D.; Muesing, M. A.; Wiskerchen, M.; Su, K. S.; Campanale, K. M.; Baxter, A. J.; Colacino, J. M. *Bioorg. Med. Chem. Lett.* **1995**, *5*, 2897−2902.
(53) Kemper, P. R.; Dupuis, N. F.; Bowers, M. T. *Int. J. Mass Spectrom.* **2009**, *287*, 46−57.
(54) Gidden, J.; Baker, E. S.; Ferzoco, A.; Bowers, M. T. *Int. J. Mass Spectrom. Ion Processes* **2005**, *240*, 183−193.
(55) Pringle, S. D.; Giles, K.; Wildgoose, J. L.; Williams, J. P.; Slade, S. E.; Thalassinos, K.; Bateman, R. H.; Bowers, M. T.; Scrivens, J. H. *Int. J. Mass Spectrom.* **2007**, *261*, 1−12.
(56) Case, D. A.; Darden, T. A.; Cheatham, I.; Simmerling, C. L.; Wang, J.; Duke, R. E.; Luo, R.; Merz, K. M.; Wang, B.; Pearlman, D. A.; et al.; *Amber-03*; University of California: San Francisco, CA, 2004.
(57) Jorgensen, W. L.; Chandrasekhar, J.; Madura, J. D.; Impey, R. W.; Klein, M. L. *J. Chem. Phys.* **1983**, *79*, 926−935.
(58) Darden, T.; York, D.; Pedersen, L. *J. Chem. Phys.* **1993**, *98*, 10089−10093.
(59) Rapport, D. C. *The Art of Molecular Dynamics Simulation*, 2nd ed.; Cambridge University Press: Cambridge, U.K., 2004.
(60) Ryckaert, J.-P.; Ciccotti, G.; Berendsen, H. J. C. *J. Comput. Phys.* **1977**, *23*, 327−341.
(61) Fraternali, F.; Cavallo, L. *Nucleic Acids Res.* **2002**, *30*, 2950−2960.
(62) Scheiner, S. *Hydrogen Bonding: A Theoretical Perspective*; Oxford University Press: New York, 1997.
(63) Bleiholder, C.; Werz, D. B.; Koppel, H.; Gleiter, R. *J. Am. Chem. Soc.* **2006**, *128*, 2666−2674.
(64) Wiesehan, K.; Stöhr, J.; Nagel-Steger, L.; Groen, T. v.; Riesner, D.; Willbold, D. *Protein Eng., Des. Sel.* **2008**, *21*, 241−246.
(65) Bitan, G.; Kirkitadze, M. D.; Lomakin, A.; Vollers, S. S.; Benedek, G. B.; Teplow, D. B. *Proc. Natl. Acad. Sci. U.S.A.* **2003**, *100*, 330−335.